JTTEE5 18:343–352
DOI: 10.1007/s11666-009-9308-3
1059-9630/$19.00 © ASM International

Quantitatively Evaluating the Effect of Oxygen/Fuel Ratio on Fe^{2+} Content in HVOF-Sprayed Ni-Zn Ferrite Coatings

Deen Zhang and D.G. McCartney

(Submitted August 25, 2008; in revised form February 15, 2009)

This article quantitatively describes the dependence of Fe^{2+} content in Ni-Zn ferrite coatings on the oxygen-fuel (O/F) ratio in high velocity oxy-fuel (HVOF) spraying. Fe^{2+} is detrimental to the magnetic properties of ferrites and should be tightly controlled. Methods were developed for calibrating energy dispersive x-ray analysis and for calculating Fe^{2+} content. The results show that the atomic percentage of the Fe^{2+} decreased from 25 to 15 at.% by increasing the O/F ratio from 80 to 110% of the stoichiometric ratio. The effect of O/F ratio has also been observed on in flight particle temperature, microstructure, and deposition efficiency. Simulations on the chemical reactions during HVOF spraying demonstrated that Fe^{2+} was produced only by the reduction of Fe^{3+} and that oxygen and zinc losses by the decomposition of ZnO in fact increased the percentage of oxygen in the coatings.

Keywords charge balance, energy dispersive x-ray (EDX) analysis, HVOF thermal spray, Ni-Zn ferrites, particle temperature

1. Introduction

Spinel soft magnetic oxides such as $(NiZn)Fe_2O_4$ and $(NiCo)Fe_2O_4$ ferrites are of great interest to the electronics industry because of their high electrical resistivity and magnetic permeability. They find a broad range of applications in telecommunications, audio and video, power transformers, magnetic storage, microelectronics, magneto-optics, microwave devices, etc. The most common method for manufacturing ferrite components is by a powder metallurgy process. There could be a number of advantages in manufacturing ferrite components by using thermal spraying processes such as high velocity oxy-fuel (HVOF) or air plasma. Costly procedures in powder metallurgy could be replaced by the direct deposition of powder onto substrates.

The chemical compositions, microstructure, and crystal structure of ferrites are extremely process sensitive; the combination of elevated temperature and gaseous atmosphere influence the magnetic properties (Ref 1). Dias and Moreira (Ref 2) reported that heating in air at 1400 °C increases zinc concentration in the outer surface when compared with the center of sintered specimens. The same results were also observed by Hellicar and Sicignano (Ref 3). Van and Johnson (Ref 4) found the opposite case with zinc loss on the surface of samples. Other authors (Ref 5, 6) reported that zinc loss in sintered ferrites leads to variations in its lattice parameter, together with changes in Fe^{2+} ion concentration and grain growth patterns. Suh and Han (Ref 7) investigated the zinc loss phenomena by monitoring the weight change of Mn-Zn ferrites in air and in nitrogen at temperatures up to 1400 °C. Weight change was not observed after heating test specimens in air from 1100 up to 1400 °C and holding for 1 h in this temperature range. Weight loss started after the atmosphere was changed from air to nitrogen at these temperatures.

Elemental variations, especially of oxygen and zinc, could become more significant during thermal spraying than would be the case in sintering processes due to the high temperature and the more complex atmosphere of the combustion gases. Yan et al. (Ref 8) investigated zinc vaporization in individual splats produced in plasma spraying and concluded that the rate of zinc loss increases with increasing surface-volume ratio. Ma and coworkers (Ref 9, 10) produced thick Ni-Zn ferrite films by using an HVOF system and observed the presence of FeO in the XRD pattern of coating which was prepared using a fuel-rich gas mixture. Better magnetic properties were obtained by using a neutral or oxygen-rich gas mixture which produced less FeO.

There could be two major reactions which cause oxygen and zinc loss and the generation of Fe^{2+} during HVOF spray of ferrite depending on the atmosphere of the flames and the particle temperature. These are the reduction of metallic ions by hydrogen and the decomposition of oxides at high flame temperatures. O/F ratio has a direct influence on the two reactions.

To understand these effects, quantitative chemical analysis based on sound methods of calibration are needed so that the analyzed composition meets the essential

Deen Zhang and **D.G. McCartney**, Department of Mechanical, Materials and Manufacturing Engineering, Faculty of Engineering, University of Nottingham, University Park, Nottingham NG7 2RD, UK. Contact e-mail: deen.zhang@nottingham.ac.uk.

requirement of charge balance between cations and anions. Energy dispersive x-ray analysis (EDX) could be considered as the most convenient method for such purpose if a method of calibration is used which is sufficiently accurate for determining light elements such as oxygen.

This article quantitatively describes the effect of O/F ratio on the Fe^{2+} content in HVOF coatings using methods for calibrating EDX data and calculating the atomic percentage of Fe^{2+}. The influence of O/F ratio on the composition, microstructure, phases present, and deposition efficiency (DE) of coatings was related to the partial pressures of combustion gases and in-flight particle temperature and velocity. The dependence of Fe^{2+} content on oxygen and zinc losses has then been studied by simulation.

2. Experimental Methods

2.1 Feed Stock Powder

Agglomerated and sintered Ni-Zn ferrite powders (FP350) was supplied by Powder Processing & Technology (PPT, Valparaiso, IN). Initial spray trials showed that the particle size of the as-supplied powder was too large for HVOF spraying and the powder was then crushed by using a high-energy puck mill and sieved to −38 μm fraction.

2.2 HVOF System and Spray Parameters

A Miller thermal/TopGun HVOF system was used for the spray trials. Powder was sprayed onto mild steel substrates, dimensions 60 ×25 × 1.88 mm. A number of coupons were clamped to a carousel which has a diameter of 250 mm and rotates around its vertical axis at 80 rpm. The tangential speed of the specimen surface relative to the flame was ~1 m s^{-1}. The gun was fixed to a traverse system which moves up and down at a velocity of 5 mm s^{-1}. Oxygen and hydrogen were used as oxidizer and fuel, respectively. The O/F ratio is expressed as the ratio used in the flame to that of the stoichiometric ratio (0.5) which is derived when hydrogen burns completely in accordance with Eq 1. A flame is fuel rich when the O/F ratio is less than unity and oxygen rich when greater than unity.

$$2H_2 + O_2 \rightarrow 2H_2O \quad \text{(Eq 1)}$$

Table 1 shows the spray parameters used for producing the four coatings and the deposition efficiencies achieved.

Table 1 HVOF spray parameters and deposition efficiency for the four coatings

Coating number	Oxygen-fuel flow rate, slpm	O/F ratio	Stand off distance, mm	Number of passes	Deposition efficiency, %
S1	253-632	0.8	150	10	33
S2	277-609	0.9	150	10	30
S3	295-590	1.0	150	10	32
S4	316-569	1.1	150	10	17

2.3 Measurements of Average In-Flight Particle Temperature and Velocity

A SprayWatch on-line diagnostic system (Oseir Ltd., Tampere, Finland) was used to monitor the temperature and velocity at different O/F ratios while the total oxygen and hydrogen flow rate was kept constant. SprayWatch produces a data point by averaging 10 captured particles and 50 data points were recorded at each test. All measurements were performed at the stand-off distance of 150 mm at which the coatings were deposited.

2.4 Characterization of Powder and HVOF Coatings

The microstructure of the powder and coatings were characterized with an ESEM-FEG scanning electron microscope (SEM) (FEI, Eindhoven, the Netherlands). The phases present in the powder and coatings were determined by x-ray diffraction using a Bruher D500 difractometer with a step size of $2\theta = 0.02$ and counting for 2 s at each step.

It is well known that an accurate quantitative determination of the oxygen content of a sample by EDX system is always problematic. Ferrite which contains about a quarter of its weight percentage as oxygen does require oxygen quantification to be reliable. An Oxford Instruments ISIS Link (ISIS) system attached to a FEI XL30 SEM was employed for analyzing the chemical composition of ferrite in association with appropriate elemental standards.

Two different errors in the EDX measurements, measurement and instrument error, were taken into account and evaluated. Measurement error or random error, which is the scatter in EDX analytical data produced on the same specimen under identical test conditions, was estimated by taking five measurements on a polished flat surface at low magnification. The mean values and sample standard deviations were calculated from the five measurements. Sample standard deviations are greater in value than standard deviations and are often used for small sample sizes. The error bands used in this article are the confidence intervals which are calculated by using the sample standard deviations at 95% confidence level.

Instrument error is an intrinsic feature of an EDX system and cannot be expressed by standard deviations. The method for calibrating instrument errors was developed based on weighted linear approximation and charge balance; the details will be discussed later.

To evaluate the reliability of EDX analysis and the method of calibration for determining oxygen content, the feed stock powder was sent to London and Scandinavian Metallurgical Co Limited (LSM) to determine the total oxygen content by using a combustion method (in equipments supplied by LECO). The principle of this method is to fuse the sample in a high-purity graphite crucible at very high temperature (up to 3000 °C) in an inert gas. The oxygen in the sample reacts with the carbon in the crucible to form CO or CO_2, which is then measured by infrared

detection. Combustion analysis of oxygen was selected as it is one of the best techniques available for accurate determination of oxygen content in oxides and that oxygen is the difficult element for EDX to quantify with acceptable accuracy.

3. Results

3.1 In-Flight Particle Temperature and Velocity

Figure 1 shows the measured temperatures and velocities using the SprayWatch system at the O/F ratios of 0.7, 0.8, 0.9, 1.0, and 1.1, with a constant standoff distance of 150 mm and total oxygen and hydrogen flow rate of 885 slpm (see Table 1). The error bars are for the confidence interval at 0.95 confidence level. The curve in Fig. 1 for velocity shows that it was only slightly affected by O/F ratios and remained in the range of 679 to 685 m s^{-1}. O/F ratio has a more significant effect on particle temperature which is 1823 °C at O/F = 0.7 but down to 1745 °C at O/F = 1.1 with the greatest drop between O/F = 1.0 and 1.1.

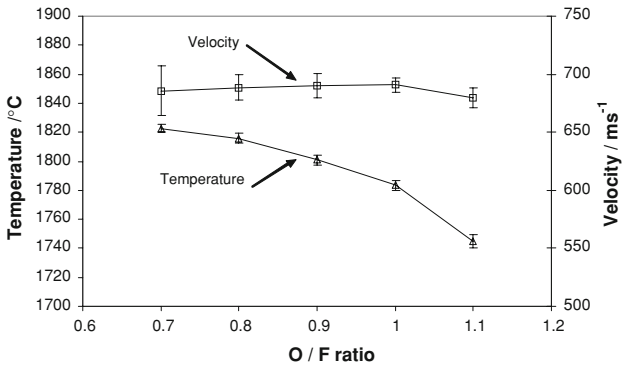

Fig. 1 Dependence of in-flight particle temperature and velocity on the O/F ratio of spray flames at a total oxygen and hydrogen flow rate of 885 slpm and a stand-off distance of 150 mm

3.2 Phases and Microstructure

Figure 2(a) to (c) shows the secondary electron (SE) images of as-received powder, polished cross section of as-received powder, and crushed powder which was used as feed stock for spraying the four coatings, respectively. Some particles greater than 38 μm can still be observed in the crushed powder. EDX analysis of the chemical composition of the powder without correction is given in Table 2 in both atomic (at.%) and weight (wt.%) percentages. From the general chemical formula for the oxide $(Ni_x, Zn_{(1-x)})_yO_yFe_{[2/3(4-y)]}O_{4-y}$, the minimum atomic percentage of oxygen of 50 at.% is obtained when $y = 4$ and the oxide becomes the bivalent FeO type. Whereas the theoretical oxygen content of 57.1 at.% for the ferrite (Fe_3O_4 type) is achieved when $y = 1$ and when the maximum oxygen content of 60 at.% is reached then $y = 0$ and the compound becomes Fe_2O_3 in type. It is obvious that the uncorrected EDX results determined 60 at.% of oxygen in Table 2 has exceeded the possible maximum for a ferrite, even though oxygen content can be any values between 57.1 and 60 at.% provided charge balance is retained, as nickel and zinc ions in the oxide are always bivalent and can be replaced by Fe^{3+}. Therefore,

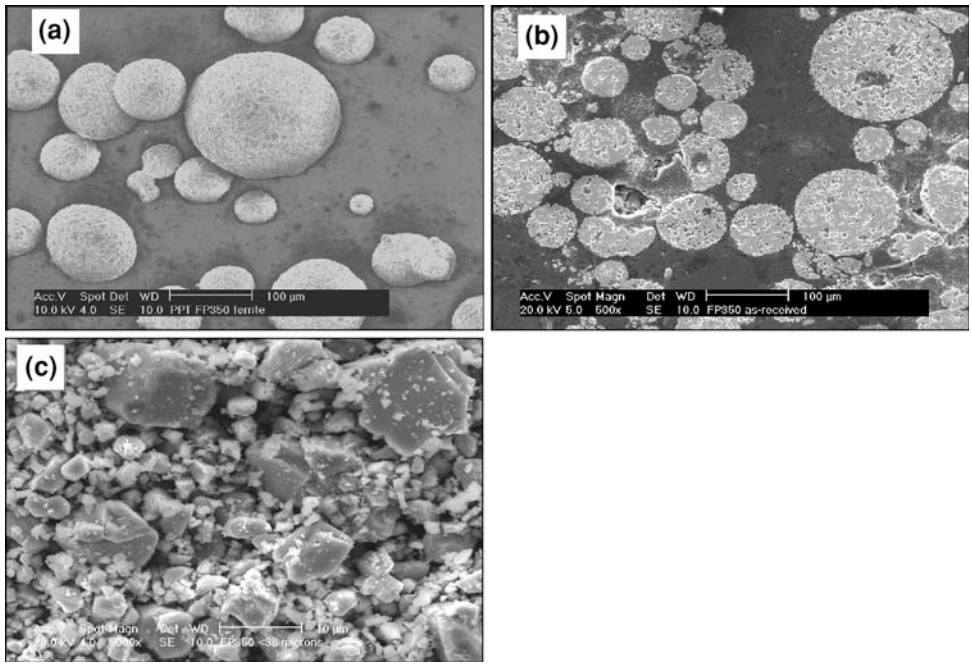

Fig. 2 SE images of the powder. (a) As received, (b) Polished cross section of (a), and (c) Powder crushed and sieved to −38 μm

Table 2 EDX and LECO analyses of FP 350 powder

	wt.%O at.%	wt.%Fe at.%	wt.%Ni at.%	wt.%Zn at.%	wt%Mn at.%
EDX as analyzed	29.53 ± 0.29 60.03 ± 0.35	52.09 ± 0.46 30.34 ± 0.36	6.70 ± 0.13 3.71 ± 0.07	10.64 ± 0.20 5.30 ± 0.09	1.05 ± 0.05 0.62 ± 0.03
EDX calibrated using Eq 2	27.79 57.98	53.37 31.90	6.86 3.90	10.91 5.57	1.07 0.65
Calibration coefficient α	+0.0342	...	...	...	...
Calibration coefficient β	...	+0.0514	+0.0514	+0.0514	+0.0514
LECO combustion analysis	27.59 (wt.%O)	...	...	...	...

the raw EDX data cannot satisfy the required charge balance.

Figure 3 depicts the back scattered electron (BSE) images of the cross sections of the four coatings at two different magnifications. The low-magnification images (Fig. 3a, c, e, g) show a similar thickness for coatings S1-S3 but a thinner S4. The deposition efficiencies (DE) of the coatings as listed in Table 1 show that the DE values for coatings S1, S2, and S3 are in the range of 30 to 33% but this value has dropped to 17% for S4. The sharp decrease of DE in coating S4 in comparison with that for coating S3 corresponds to the significant reduction of particle temperature (see Fig. 1), which determines the cut off diameter of deposited particles. All coatings were dense and there was no evidence of debonding from the substrates. The micrographs at higher magnification (Fig. 3b, d, f, h) reveal that there is a compositional contrast in coatings S1 and S2 (Fig. 3b, d) with darker internal areas in solid particles and brighter fringes surrounding them (see the particles arrowed in Fig. 3b, d). The brighter areas also take a large proportion of the melted splats. Semiquantitative EDX spot analyses detected lower oxygen and zinc contents in the brighter fringes than in the darker center of unmelted particles. A reliable EDX quantification could not be conducted on these fringes because of their limited size. Such compositional contrast cannot be observed in coatings S3 and S4 (Fig. 3f, h) although the main constituents in these coatings are also melted splats. The nature of the compositional contrast and the reasons for it will be discussed in the following sections.

Uncalibrated EDX-determined mean values and confidence intervals of the chemical compositions of the coatings are given in Table 3. In comparison with the composition of the powder (Table 2), S1 with the lowest O/F ratio had lost about 4 at.% oxygen and 4.4 at.% zinc. Coatings S2, S3, and S4 lost about 2.4 at.% oxygen and 4.2 to 4.4 at.% zinc. The mean values of iron contents decreased with increasing O/F ratio from 39.4 at.% in S1 down to 36.2 at.% in S4, representing an iron gain on all samples in the range from 5.9 to 9.1 at.% when compared with the powder. Such comparisons between powder and coating compositions are acceptable as relative values, as all were analyzed with the same instrument but it has to be realized that these values contained instrument errors and could not be used for estimating FeO contents. O/F ratios can be seen to have a significant effect on the variation of the chemical compositions with coating S1 suffered the greatest loss of zinc and oxygen owing to the fuel-rich atmosphere in which it was sprayed.

Figure 4 shows the XRD patterns of the powder and the coatings. The diagram is divided for clarity into part (a) and (b) with 2θ ranges 26 to 48° and 48 to 92°, respectively. The diffraction lines of (Ni Zn)Fe_2O_4, $Fe_{0.9536}O$, and Fe_3O_4 from the JCPDS data base are also included for reference. It is seen that the reference lines for (Ni Zn)Fe_2O_4 and Fe_3O_4 were all overlapping except a single low-intensity Fe_3O_4 diffraction peak at $2\theta = 75.0$ and two low-intensity lines of (Ni Zn)Fe_2O_4 at $2\theta = 33.2$ and 82.0, respectively. The powder had a peak at $2\theta = 75.0$, indicating that a small proportion of Fe_3O_4 may be present in the powder. The Fe_3O_4 peaks were not clearly seen in the coatings due to peak broadening.

All coatings contained low-intensity peaks of wustite $Fe_{1-x}O$. These peaks match better with the JCPDS lines of $Fe_{0.9536}O$ than with the stoichiometric FeO. The wustite peaks in the lowest O/F ratio coating, S1, were very close to the reference lines at $2\theta = 42.2$ and 61.2 but the diffraction peaks gradually shifted away from the JCPDS lines in the order S2, S3, and S4,. The stronger FeO peaks for coatings S1 and S2 can be related to the brighter areas in Fig. 3(b) and (d). The weaker FeO peaks in coatings S3 and S4 suggest less Fe^{2+} and more homogenous distribution of oxygen in the two coatings (see Fig. 3f, h). Peak broadening could be seen in the XRD patterns of all coatings in comparison with those for the powder which can be attached to a combination of fine grain size and microstrain.

3.3 Calibrated EDX Analysis of Composition

The effect of instrument errors was mainly on the mean values of EDX measurements. The essential requirement for ferrite materials used for calibrating the instrument error of the EDX systems was that it did not contain Fe^{2+}, i.e., all iron ions were Fe^{3+} and all other cations were bivalent. The feed stock powder was considered suitable as its XRD pattern shown in Fig. 4 did not reveal any evidence of FeO.

Assuming that the errors in the EDX-determined compositions were mainly caused by the inaccurate analysis of oxygen, a weighted linear approximation was applied to the calibration process. This method

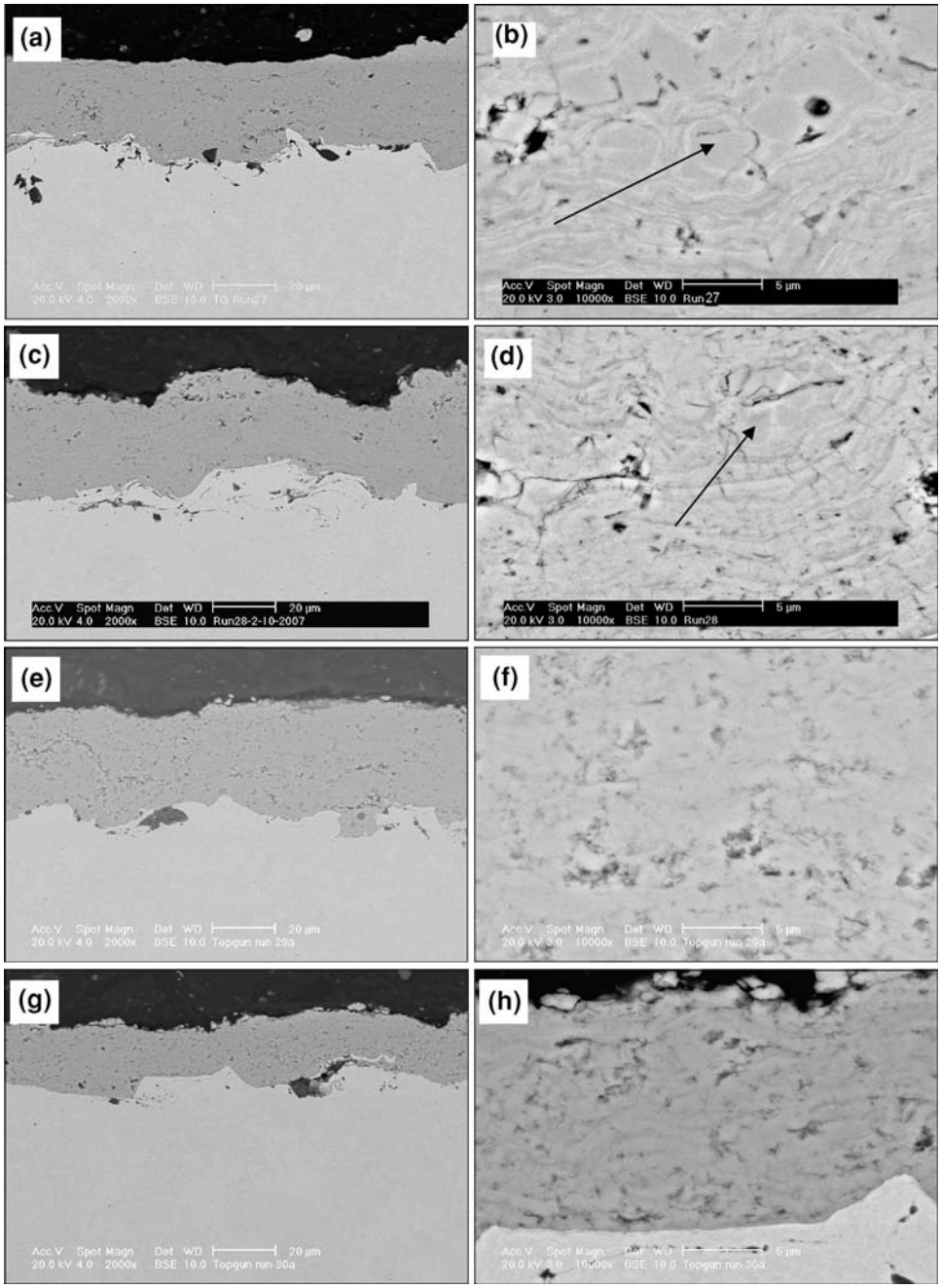

Fig. 3 BSE images of cross sections of coatings S1 (a, b), S2 (c, d), S3 (e, f), and S4 (g, h). Arrows point to the unmelted particles with brighter fringes

Table 3 Original EDX analyses of the four HVOF coatings

Coating number	wt.%O at.%	wt.%Fe at.%	wt.%Ni at.%	wt.%Zn at.%	wt.%Mn at.%
S1	26.49 ± 0.20	65.22 ± 1.1	5.28 ± 0.45	1.67 ± 0.68	1.33 ± 0.04
	55.88 ± 0.27	39.41 ± 0.67	3.04 ± 0.26	0.86 ± 0.35	0.81 ± 0.02
S2	27.86 ± 0.10	64.26 ± 0.58	4.97 ± 0.18	1.64 ± 0.37	1.27 ± 0.09
	57.57 ± 0.11	38.04 ± 0.29	2.80 ± 0.11	0.83 ± 0.30	0.76 ± 0.06
S3	27.99 ± 0.23	63.77 ± 0.51	5.14 ± 0.14	1.86 ± 0.34	1.23 ± 0.10
	57.74 ± 0.29	37.69 ± 0.40	2.89 ± 0.09	0.94 ± 0.17	0.74 ± 0.06
S4	27.89 ± 0.17	62.59 ± 1.17	6.03 ± 0.13	2.22 ± 0.93	1.27 ± 0.04
	57.65 ± 0.24	37.07 ± 0.65	3.40 ± 0.07	1.06 ± 0.38	0.77 ± 0.02

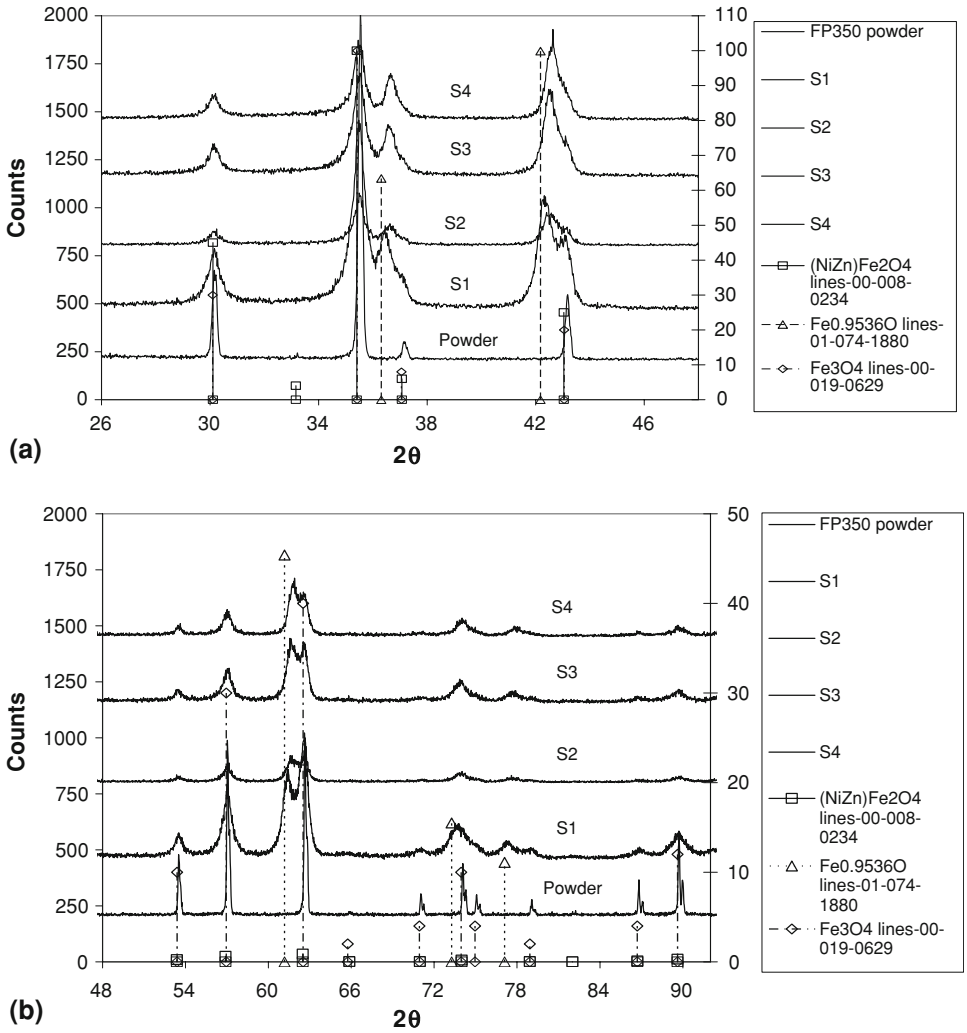

Fig. 4 XRD patterns of the powder and the four coatings

supposed that oxygen content had been over or under estimated by a percentage α and the metals were consequently under or over estimated by a percentage β of their measured values, the atomic percentages of elements in the powder must satisfy two conditions, i.e., charge balance and summing up to 100%. These were expressed in Eq 2.

$$\begin{aligned}&\text{at\%O}(1-\alpha)\\&=\frac{3\,\text{at\%Fe}(1+\beta)+2(1+\beta)(\text{at.\%Ni}+\text{at.\%Zn}+\text{at.\%Mn})}{2}\\&\text{at\% O}(1-\alpha)+(1+\beta)\\&\times(\text{at.\%Fe}+\text{at.\%Ni}+\text{at.\%Zn}+\text{at.\%Mn})=100\end{aligned}\qquad\text{(Eq 2)}$$

from which α and β were worked out by applying the EDX-measured mean atomic percentages (at.%) as given in Table 2. The corrected composition CPat.% of the powder was then calculated by using Eq 3.

$$\begin{aligned}\text{CPat.\%O}&=\text{at.\%O}(1-\alpha)\\\text{CPat.\%Fe}&=\text{at.\%Fe}(1+\beta)\\\text{CPat.\%Ni}&=\text{at.\%Ni}(1+\beta)\\\text{CPat.\%Zn}&=\text{at.\%Zn}(1+\beta)\\\text{CPat.\%Mn}&=\text{at.\%Mn}(1+\beta)\end{aligned}\qquad\text{(Eq 3)}$$

The calibrated composition and the values of α and β of the powder are given in Table 2. It is seen that the calibrated atomic percentage of oxygen was slightly greater than 57.1 at.% which is the theoretical value for a stoichiometric ferrite. The calibrated weight percentages in Table 2 were obtained by conversion from the calibrated EDX atomic percentages. The LECO combustion method was used to determine the oxygen content and gave a value of 27.59 wt.% O (see Table 2). This compares favorably with the calibrated EDX value of 27.79 wt.% O. The close agreement between the calibrated EDX oxygen content and that produced by LECO analysis

Table 4 Calculated compositions of the coatings using Eq 5 and the factor γ

Coating number	CCat.%O	CCat.%Fe	CCat.%Ni	CCat.%Zn	CCat.%Mn	at.%Fe^{2+}	at.%Fe^{3+}
S1	53.87	40.89	3.26	0.97	0.91	25.21	15.68
S2	55.50	39.47	3.00	0.94	0.86	17.01	22.46
S3	55.66	39.11	3.10	1.06	0.84	16.01	23.10
S4	55.57	38.46	3.65	1.20	0.87	15.68	22.78
γ	−3.60%	+3.76%	+7.28%	+12.83%	+12.90%	...	...

demonstrates the precision of the calibration procedure for the EDX analysis in the important case of oxygen.

The next operation was to estimate the differences between the calibrated composition and the original EDX measurement of the powder to define the range of calibrations for the compositions of the HVOF coatings. The calibrating factor γ was estimated by using Eq 4:

$$\gamma = (\text{the calibrated atomic percentage} - \text{EDX measurement})/\text{EDX measurement} \quad \text{(Eq 4)}$$

The derived γ values for the elements are given in Table 4 where the positive and negative signs were applied together with γ. Note that γ was not a factor of single value but had a separate value for each element.

With the γ values known, the compositions of the four coatings, CCat.%, can now be calibrated by using Eq 5:

$$\begin{aligned} \text{CCat.\%O} &= \text{at.\%O}(1+\gamma) \\ \text{CCat.\%Fe} &= \text{at.\%Fe}(1+\gamma) \\ \text{CCat.\%Ni} &= \text{at.\%Ni}(1+\gamma) \\ \text{CCat.\%Zn} &= \text{at.\%Zn}(1+\gamma) \\ \text{CCat.\%Mn} &= \text{at.\%Mn}(1+\gamma) \end{aligned} \quad \text{(Eq 5)}$$

where at.% were the original EDX atomic percentages as shown in Table 2 and CCat.% were the calibrated compositions of the coatings. The results of calibrations are shown in Table 4.

There may be small deviations from summing up to 100% in the calibrated compositions given in Table 4. These deviations were tolerable as they did not significantly affect the evaluations of Fe^{2+} contents.

3.4 Estimation of Fe^{2+} Contents in the HVOF Coatings

The atomic percentages of the bivalent and trivalent iron ions in the coatings were calculated by using Eq 6 which was based on charge balance.

$$\text{CCat\%O} = \frac{2(\text{at.\%Fe}^{2+} + \text{CCat.\%Ni} + \text{CCat.\%Zn} + \text{CCat.\%Mn}) + 3\,\text{at.\%Fe}^{3+}}{2} \quad \text{(Eq 6)}$$

$$\text{at.\%Fe}^{2+} + \text{at.\%Fe}^{3+} = \text{CCat.\%Fe}$$

where at.%Fe^{2+} and at.%Fe^{3+} are, respectively, the atomic proportions of Fe^{2+} and Fe^{3+} ions to be calculated and CCat.% were the calibrated compositions of the coatings as shown in Table 4.

The last two columns in Table 4 show the calculated values for at.%Fe^{2+} and at.%Fe^{3+}. It is seen that the atomic percentages of at.%Fe^{2+} decreased from 25.2.at% in coating S1 which was sprayed in a fuel-rich flame to 15.7.at% in coating S4 which was produced with an oxygen-rich flame. The greatest drop in at.%Fe^{2+} content occurred between coatings S1 and S2.

3.5 Simulation of the Effect of Losing Zinc and Oxygen on the Overall Composition and Fe^{2+} Content

The calibrated composition of the powder given in Table 2 was the best starting composition for the simulations as it contained no Fe^{2+} and all coatings were sprayed from it. The atomic percentages of elements had first to be converted to molar numbers. The molar number of oxygen in the powder was selected as MO = 4.00. The rest were calculated as MFe = 2.18, MNi = 0.28, MZn = 0.41, and MMn = 0.048. The simulated compositions, which were designated as Sat.%, after losing δ moles of oxygen and ε moles of zinc from the starting composition were expressed as:

$$\begin{aligned} \text{Sat.\%O} &= \frac{\text{MO}-\delta}{(\text{MO}-\delta)+\text{MFe}+\text{MNi}+(\text{MZn}-\varepsilon)+\text{MMn}} \\ \text{Sat.\%Fe} &= \frac{\text{MFe}}{(\text{MO}-\delta)+\text{MFe}+\text{MNi}+(\text{MZn}-\varepsilon)+\text{MMn}} \\ \text{Sat.\%Ni} &= \frac{\text{MNi}}{(\text{MO}-\delta)+\text{MFe}+\text{MNi}+(\text{MZn}-\varepsilon)+\text{MMn}} \\ \text{Sat.\%Zn} &= \frac{\text{MZn}-\varepsilon}{(\text{MO}-\delta)+\text{MFe}+\text{MNi}+(\text{MZn}-\varepsilon)+\text{MMn}} \\ \text{Sat.\%Mn} &= \frac{\text{MMn}}{(\text{MO}-\delta)+\text{MFe}+\text{MNi}+(\text{MZn}-\varepsilon)+\text{MMn}} \end{aligned} \quad \text{(Eq 7)}$$

The same moles of oxygen and zinc were lost when δ = ε, i.e., in the form of ZnO. Table 5 shows the simulated atomic percentages using Eq 7 at given δ = ε values. The simulated atomic percentage of Fe^{2+} and Fe^{3+} which were designated as Sat.%Fe^{2+} and Sat.%Fe^{3+}, respectively, were calculated by applying the simulated Sat.% values to

Table 5 Simulated Sat.%Fe^{2+}, Sat.%Fe^{3+}, and other elements at given δ = ε values

δ = ε mole	Sat.%O	Sat.%Fe^{2+}	Sat.%Fe^{3+}	Sat.%Ni	Sat.%Zn	Sat.%Mn
0.00	57.87	0	31.48	3.98	5.98	0.70
0.1	58.11	0	32.42	4.07	4.69	0.70
0.2	58.36	0	34.42	4.19	3.30	0.72
0.3	58.63	0	34.48	4.33	1.82	0.74
0.4	58.91	0	35.61	4.47	0.25	0.77
0.415	58.95	0	35.78	4.49	0	0.77

Table 6 Simulated compositions for coatings S1 and S4 at ε = 0.35 and δ > ε

ε = 0.35	Sat.%O SMO	Sat.%Fe^{2+} SMFe^{+2}	Sat.%Fe^{3+} SMFe^{+3}	Sat.%Ni SMNi	Sat.%Zn SMZn	Sat.%Mn SMMn	Simulated coatings
δ = 1.05	53.51	25.42	14.05	4.99	1.15	0.88	S1
	2.95	1.40	0.775	0.275	0.086	0.06	
δ = 0.8	55.53	15.65	22.13	4.77	1.10	0.84	S4
	3.2	0.90	1.275	0.275	0.08	0.06	

Eq 6 in the place of calibrated compositions CCat.%. Table 5 shows that losing ZnO increased the atomic percentages of all elements including oxygen except zinc which decreased. The atomic percentages of Sat.%Fe^{2+} remained at zero at all given values of δ = ε.

Starting from the calibrated composition of the powder and assuming δ > ε, Table 6 shows the atomic percentages of all elements calculated using Eq 7 with δ = 1.05 and δ = 0.8, respectively, and a fixed ε = 0.35. The atomic proportions of Sat.%Fe^{2+} and Sat.%Fe^{3+} were then calculated using Eq 6 and the simulated atomic percentages as given in Table 6. The results depict that the composition at δ = 1.05 was close to that of coating S1 (see Table 2) and to coating S4 at δ = 0.8. The corresponding molar numbers of the elements are also tabulated in Table 6, with SMN (standing for the simulated molar number) prefixing the name of the elements.

δ in Table 6 can be considered as consisting of two parts, i.e., 0.35 moles were lost in the form of ZnO and δ − 0.35 moles due to the reduction of Fe^{3+} to Fe^{2+}. The molar loss of oxygen from the reduction was therefore 1.05 − 0.35 = 0.7 for simulated coating S1 and 0.8 − 0.35 = 0.45 for coating S4. It is interesting to note by comparing these values with the molar numbers of SMN Fe^{2+} = 1.4 for S1 and SMN Fe^{2+} = 0.9 for S4 that two moles of Fe^{2+} were produced with every one mole of oxygen loss either by reacting with hydrogen or by the reduction of Fe^{3+} to Fe^{2+} at high temperature.

The results of simulation given in Table 5 and 6 proved that the reduction of Fe^{3+} to Fe^{2+} was the only cause for oxygen loss and the generation of Fe^{2+}.

4. Discussion

Spinel structure is named after the mineral *spinel* ($MgAl_2O_4$) with the stoichiometric composition AB_2O_4. It is essentially *cubic,* with 32 O^- ions forming a fcc lattice unit cell. The cations (usually metals) occupy 1/8 of the tetrahedral sublattice commonly designated as site A and 1/2 of the octahedral sublattice (site B). Spinel is very flexible with respect to the cations it can incorporate; there are over 100 known compounds (Ref 11). In particular, the A and B cations can mix, i.e., the composition with respect to one unit cell can be: (A_8) (B_{16}) O_{32}, A_8 (B_8A_8) O_{32} = $A(AB)O_4$ or $(A_{16/3}B_{16/3})$ $(A_{16/3}B_{32/3})$ O_{32}. In many cases, the spinel structure contains voids at the sublattices for cations, making them off-stoichiometric compositions with balanced charges. It is the high flexibility that makes ferrite sensible to processing parameters.

The splats in coatings S1 and S2, as shown in Fig. 3(b) and (d), are well defined by the presence of compositional contrast but such BSE contrast cannot be observed in the microstructure of coatings S3 and S4 (see Fig. 3f, h). The difference in the microstructure between the two groups of coatings can be related to the two major chemical reactions, i.e., the reduction of oxides when free hydrogen was present (O/F < 1):

$$Fe_2O_{3(s)} + H_{2(g)} \leftrightarrow H_2O_{(g)} + 2FeO_{(s)} \quad \text{(Eq 8a-1)}$$

$$\text{with} \quad K_p = \frac{P_{H_2O}}{P_{H_2}} \quad \text{(Eq 8a-2)}$$

$$ZnO_{(s)} + H_{2(g)} \leftrightarrow Zn_{(g)} + H_2O_{(g)} \quad \text{(Eq 8b-1)}$$

$$\text{with} \quad K_p = \frac{P_{H_2O} \cdot P_{Zn}}{P_{H_2}} \quad \text{(Eq 8b-2)}$$

and the following reactions which can take place due to the instability of Fe^{3+} and Zn^{2+} at elevated temperatures at both O/F < 1 and O/F > 1.

$$2Fe_2O_{3(s)} \leftrightarrow 4FeO_{(s)} + O_{2(g)} \quad \text{(Eq 9a-1)}$$

$$\text{with} \quad K_p = P_{O_2} \quad \text{(Eq 9a-2)}$$

$$ZnO_{(s)} \leftrightarrow Zn_{(g)} + 0.5O_{2(g)} \quad \text{(Eq 9b-1)}$$

$$\text{with} \quad K_p = P_{O_2}^{0.5} \cdot P_{Zn} \quad \text{(Eq 9b-2)}$$

where P_{H_2O}, P_{O_2}, etc. are the partial pressures of the gases and K_p values are the equilibrium constants for each reaction.

The equilibrium constants shown in Eq 8a-2 and 8b-2 indicate that the forward reactions 8a-1 and 8b-1 can proceed when the partial pressure of hydrogen is greater than its equilibrium pressure P_{H_2}. Reducing hydrogen partial pressure by increasing O/F ratio can stop or even reverse these reactions. The reaction given in 8a-1 is exothermic while that in 8b-1 is endothermic. The two reactions would therefore behave in different ways when a temperature change takes place.

Reactions 9a-1 and 9b-1 are both endothermic but the equilibrium constant given by 9a-2 is determined only by the oxygen partial pressure; 9b-2 is also affected by the partial pressures of zinc and oxygen. Both reactions could be stopped or reversed by increasing oxygen partial pressure or the O/F ratio.

It has to be emphasized, however, that O/F ratio does not only affect the partial pressures of oxygen and hydrogen but also the temperature and velocity of particles in flight (see Fig. 1). The fact that there are brighter fringes to be found in the microstructure in Fig. 3(d) but not in 3(f) demonstrates differences in oxygen contents between coatings S2 and S3. This indicates the effect of a higher hydrogen partial pressure in the microstructure and chemical composition of coating S2. It should be noted that there was only a small differences of 18 °C between the particle temperatures found in coatings S2 and S3 (see Fig. 1).

The DE values shown in Table 1 and the particle temperature shown in Fig. 1 indicate that there is a temperature below which the DE value will drop sharply for the powder used in this investigation. It is interesting to notice that the ratio between the molar numbers of Fe^{2+} produced and the oxygen consumed (8a-1) or released (9a-1) is 2:1. This is in good agreement with the data listed in Table 6.

Zinc and iron existed in the spinel structure as Zn^{2+} and Fe^{3+} ions. To be decomposed, the metallic ions had to gain electrons from O^{2-} ions to become atoms. O^{2-} became atom by losing electrons. This process was equivalent to the decomposition of zinc or iron oxide even though metallic and oxygen ions in the spinel structure were not in the form of ZnO or Fe_2O_3. As can be seen in Table 5 that all elements including oxygen but except zinc increased their proportions with increasing δ values when $\delta = \varepsilon$ and no Fe^{2+} was generated even though the molar numbers of oxygen were actually reduced. This is simply because the loss of ZnO did not alter the charge balance or the relative ratios between O^{2-} and Fe^{3+} in the ferrite or in another word, losing ZnO increased the atomic percentage of the trivalent oxide Fe_2O_3 and hence the oxygen content.

There would be less Fe^{2+} than is shown in Table 6 if part of the oxygen from decomposed ZnO was retained and used to compensate the oxygen loss due to the reduction of Fe^{3+} to Fe^{2+}. The good agreement between the calibrated EDX analyses of coatings S1 and S4 given in Table 2 and the simulated compositions listed in Table 6 suggests that the decomposition of ZnO has contributed negligible amount of oxygen to the overall oxygen contents in the coatings. The conclusion that losing ZnO was irrelevant to the generation of Fe^{2+} has also been demonstrated by Liang et al. (Ref 12) who reported the presence of Fe^{2+} in air plasma-sprayed Ni-Co ferrite in which no metals could be vaporized.

The 25 at.%Fe^{2+} in coating S1 as shown in Table 4 is equivalent to over 50 at.%FeO if all Fe^{2+} had been tied up in the wustite phase. The magnitude of the diffraction peaks of FeO in the XRD pattern as shown in Fig. 4 did not seem to match with such a large proportion of FeO phase. It is believed that most of the Fe^{2+} ions still remained inside the spinel lattice and only a small fraction had formed FeO, most probably at the outside layer of melted splats and unmelted particles such as the brighter fringes shown in Fig. 3(b) and (d). Morineau and Paulus' (Ref 13, 14) research into the effect of oxygen partial pressure on the distribution of ions on the sublattice of manganese ferrites showed that over 3.0 at.%Fe^{2+} could reside in the octahedral site (B site) in the spinel structure where the majority of Fe^{3+} ions took up occupancy.

The very close agreement between the LECO analysis and the calibrated EDX data on the oxygen content of the powder shown in Table 2 demonstrated that Eq 2 used for calibrating the EDX analysis is satisfactory for evaluating the full analysis of the powder and the coatings. This method can also be used in other processes where zinc and oxygen content may vary.

5. Conclusions

a. HVOF-sprayed coatings could contain up to 25.2 at.% Fe^{2+} under the conditions used in the current investigation. The proportion of Fe^{2+} can be significantly reduced by increasing the O/F ratio of the combustion gases.

b. O/F ratio has a significant influence on particle temperature but not on the particle velocity.

c. The analytical method developed based on charge balance and weighted linear approximation has been shown by LECO combustion analysis of oxygen in the powder to be very satisfactory for calibrating the EDX analysis of ferrite materials.

d. Simulated compositions which were very close to the calibrated EDX analyses of the coatings showed that zinc and part of oxygen were lost in the form of ZnO, which increased the oxygen percentage but did not generate any Fe^{2+}.

e. The reduction of Fe^{3+} to Fe^{2+} brought about by the spraying conditions, in particular the reduction in O/F ratio, promotes a release of oxygen resulting in the decrease in the atomic percentage of oxygen and an increase in Fe^{2+} in the sprayed ferrite coatings.

Acknowledgments

The authors wish to thank the EC for financial support (Contract No. COOP-CT-2006-031944). Specifically, the authors are grateful to Dr. J. Yellup, University of Nottingham and Dr. I. Linden, Oseir Ltd. (for SprayWatch

measurements) as well as to Prof. S. J. Harris for valuable comments on the manuscript.

References

1. K. Ishino and Y. Narumiya, Development of Magnetic Ferrites—Control and Application of Losses, *Am. Ceram. Soc. Bull.*, 1987, **66**(10), p 1469-1474
2. A. Dias and R.L. Moreira, Chemical Mechanical and Dielectric Properties after Sintering of Hydrothermal Nickel-Zinc Ferrites, *Mater. Lett.*, 1999, **39**, p 69-76
3. N.J. Hellicar and A. Sicignano, Dynamic Role of Zinc-Oxide in the Sintering of Manganese Zinc Ferrites, *Am. Ceram. Soc. Bull.*, 1982, **61**(4), p 502-505
4. M.F. Van and D.W. Johnson, Jr., Impurity-Induced Exaggerated Grain-Growth in Mn-Zn Ferrites, *J. Am. Ceram. Soc.*, 1978, **61**(7-8), p 342-349
5. K. Majima, M. Hasegawa, S. Katsuama, H. Nagai, and S. Mishima, ZnO Precipitation During Sintering of Ni-Zn Ferrite Used for the Substrate of Thin-Film Heads, *J. Mater. Sci. Lett.*, 1993, **12**(3), p 185-187
6. K. Majima, M. Hasegawa, M. YoKota, H. Nagai, and S. Mishima, Microstructural Control of Ni-Zn Ferrite for Thin-Film Heads, *Mater. Trans. JIM*, 1993, **34**(6), p 556-562
7. J.J. Suh and Y.H. Han, Quantitative Analysis of Zinc Vaporization from Manganese Zinc Ferrites, *J. Am. Ceram. Soc.*, 2003, **86**(5), p 765-768
8. Q. Yan, R.J. Gambino, S. Sampath, L.H. Lewis, L. Li, E. Baumberger, A. Vaidya, and H. Xiong, Effects of Zinc Loss on the Magnetic Properties of Plasma-Sprayed MnZn Ferrites, *Acta Mater.*, 2004, **52**(11), p 3347-3353
9. X. Ma, S. Ge, T. Zhang, and Y. Zhang, *Thermal Spray 2003: Advancing the Science and Applying the Technology*, C. Moreau and B. Marple, Eds., ASM International, Materials Park, OH, 2003, p 841
10. S. Ge, X. Ma, T. Zhang, M. Wu, H. Zhang, and Y.D. Zhang, Structural and Magnetic Properties of Nanostructured NiO.5Zno.5Fe_2O_4 Films Fabricated by Thermal Spray, *J. Appl. Phys.*, 2003, **93**(10), p 7498-7500
11. N.N. Greenwood, *Ionic Crystals, Lattice Defects and Non-Stoichiometry*, Butterworths, London, 1968
12. S. Liang, B.G. Ravi, S. Sampath, and R.J. Gambino, Atmospheric Plasma Sprayed Cobalt Ferrite Coatings for Magnetostrictive Sensor Applications, *IEEE Trans. Magn.*, 2007, **43**(6), p 2391-2393
13. R. Morineau and M. Paulus, Oxygen Partial Pressures of Mn-Zn Ferrites, *Phys. Status Solidi (a)*, 1973, **20**, p 373-380
14. R. Morineau, Structural Defects and Oxidation-Reduction Equilibrium in Mn, Zn Ferrites, *Phys. Status Solidi (a)*, 1976, **38**, p 559-568